PROCEEDINGS A

rspa.royalsocietypublishing.org

Research

Cite this article: Zhang Y, Lu B, Lü C, Feng X. 2017 Theory of energy harvesting from heartbeat including the effects of pleural cavity and respiration. *Proc. R. Soc. A* **473**: 20170615.
http://dx.doi.org/10.1098/rspa.2017.0615

Received: 6 September 2017
Accepted: 25 October 2017

Subject Areas:
mechanical engineering

Keywords:
energy harvesting, heartbeat, respiration, flexible electronics, scaling law

Author for correspondence:
Chaofeng Lü
e-mail: lucf@zju.edu.cn

Theory of energy harvesting from heartbeat including the effects of pleural cavity and respiration

Yangyang Zhang[1], Bingwei Lu[2], Chaofeng Lü[1,3,4] and Xue Feng[2]

[1]Department of Civil Engineering, Zhejiang University, Hangzhou 310058, People's Republic of China
[2]Department of Engineering Mechanics, Tsinghua University, Beijing 100084, People's Republic of China
[3]Key Laboratory of Soft Machines and Smart Devices of Zhejiang Province, and [4]Soft Matter Research Center, Zhejiang University, Hangzhou 310027, People's Republic of China

CL, 0000-0003-2846-1266

Self-powered implantable devices with flexible energy harvesters are of significant interest due to their potential to solve the problem of limited battery life and surgical replacement. The flexible electronic devices made of piezoelectric materials have been employed to harvest energy from the motion of biological organs. Experimental measurements show that the output voltage of the device mounted on porcine left ventricle in chest closed environment decreases significantly compared to the case of chest open. A restricted-space deformation model is proposed to predict the impeding effect of pleural cavity, surrounding tissues, as well as respiration on the efficiency of energy harvesting from heartbeat using flexible piezoelectric devices. The analytical solution is verified by comparing theoretical predictions to experimental measurements. A simple scaling law is established to analyse the intrinsic correlations between the normalized output power and the combined system parameters, i.e. the normalized permitted space and normalized electrical load. The results may provide guidelines for optimization of *in vivo* energy harvesting from heartbeat or the motions of other biological organs using flexible piezoelectric energy harvesters.

THE ROYAL SOCIETY PUBLISHING

1. Introduction

Implantable devices, aiming to solve problems such as heart failure, obesity, blood pressure control, wound healing, neural-stimulation and drug delivery, have made significant progress in clinical applications in recent years [1–5]. Pacemakers and implantable cardioverter defibrillators (ICDs) are most commonly used among these devices mentioned above. Both pacemakers and ICDs need a replacement every several years for various reasons, e.g. end of the battery life [6]. This needs additional surgeries which may bring a notable complication risk, especially in the case of involving lead additions [7]. On the other hand, these surgeries and device replacements are costly and apt to bring additional injuries to patients. However, the development of currently available battery technology is much slower than the electronic devices, which limits the pace of improvement in design and functionality of implantable electronic devices.

Self-powered implantable devices provide a potential way to address the shortcomings of battery replacement problem of implantable devices with the breakthrough technology of energy harvesting from ambient environments [8–13]. The main mechanical energy scavenging strategies are to harvest energy from biomechanical motions of human organs, such as heart-beating, blood flow and breathing etc. Lead zirconate titanate (PZT) is the mostly used material in mechanical energy harvesters (MEHs) for its high piezoelectric coefficients, and flexible/stretchable electronics with PZT material were studied intensively by Huang's group [14–18]. Based on these mechanical strategies, Dagdeviren *et al.* demonstrated a conformal device to collect electric power from motions of porcine heart, lung or diaphragm based on a flexible PZT MEH [19]. Ansari *et al.* [20] designed a fan-folded structure consisting of bimorph PZT beams for powering biomedical devices and sensors inside the body. Other piezoelectric materials, e.g. zinc oxide (ZnO), PMN-PT or PVDF, were also resorted to fabricate flexible MEHs [21–23]. For example, people may generate electric power using a flexible PVDF piezoelectric generator from the pulsation of ascending aorta of a swine or employing a ZnO breathing-driven implanted triboelectric nanogenerator powered by the rat's diaphragm [24–26].

Most recently, Lu *et al.* conducted a set of experiments to invest energy harvesting from the porcine heartbeat using flexible PZT MEH [27], in which the output voltage was measured under various conditions, i.e. chest open, chest closed and awake from anaesthesia. When the device is mounted on the heart surface in a matter of covering from the apex of the left ventricle (LV) to the right ventricle, the peak-to-valley amplitude of the output voltage reduces from 1.91 V with chest open to 1.09 V with chest closed, i.e. a reduction of 50%, while the average power is 0.02 µW with chest open to 0.005 µW with chest closed, i.e. a reduction of 75%. To demonstrate the underlying mechanism of the reduction in energy harvesting in chest closed environment relative to chest open, Zhang *et al.* [28] proposed a nonlinear compressive spring model to account for the impeding effects of surrounding tissues on the energy harvesting efficiency of the electromagnetic harvesting device. They treated the surrounding tissues, including the pericardium serosa, pleura and lung, approximately as a homogeneous medium that posed impeding effects on the deformation of the device. That is, once deformed, the device will be impeded by the spring. However, the anatomy shows that the cavum is enveloped by the visceral and parietal layer of the pericardium and that a gap of 5–10 mm exists between the parietal layer and the pleura [29]. As a result, the device may deform freely at its early stage and will be impeded only if the deformation amplitude exceeds this gap. In addition, the back-and-forth deformation of the device will also vary with respiration as the chest is closed.

In this paper, we propose a restricted deformation space model to demonstrate this mechanism of energy harvesting efficiency reduction in chest closed environment based on an electromechanical analysis. An analytical solution for the output voltage and power has been derived and will be validated by comparing with experimental measurements. A simple scaling law will be established which reveals the dependence of the normalized electric outputs on the normalized permitted space and the normalized electrical load. The output power can be tuned and optimized according to this scaling law by choosing properly the material, geometric and

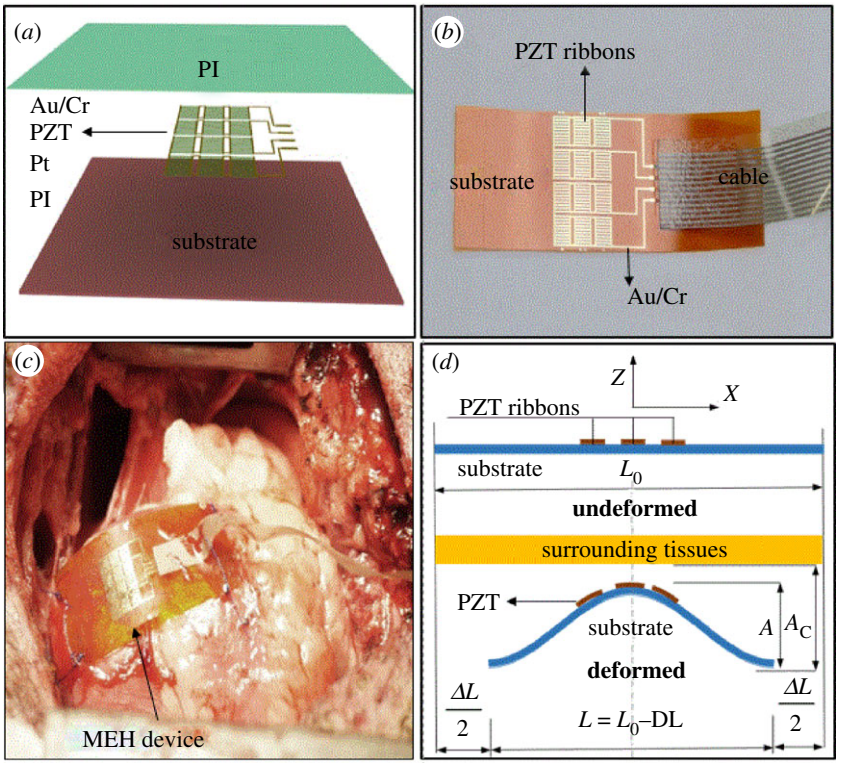

Figure 1. (*a*) Schematic illustration of layered structure of the flexible PZT MEH. (*b*) Photograph of the MEH device connected with cables. (*c*) Photograph of the MEH device that is mounted on the surface of the heart with chest open. (*d*) Schematic diagram of the device deformation with constraints of surrounding tissues.

circuit parameters of the energy harvesting system. The results can also provide design guidelines for similar MEH devices that are applied in other biological environments.

2. Mechanical analyses of the mechanical energy harvester device

The PZT MEH is a layered structure (figure 1*a*), where PI (thickness ~ 1.2 µm, $E = 8.55$ GPa) serves as the adhesive layer, Pt (thickness ~ 0.3 µm, $E = 196$ GPa) serves as the bottom electrode, then PZT ribbons (length ~ 2.2 mm, width ~ 100 µm, thickness ~ 500 nm, $E = 128$ GPa) serve as the functional layer which can generate electric power under deformation, Au (thickness ~ 0.2 µm, $E = 97$ GPa) and Cr (thickness ~ 10 nm, $E = 292$ GPa) serve as the top electrode and PI (thickness ~ 1.2 µm, $E = 8.55$ GPa) serves as the top protective layer. Lithography and wet etching methods were employed to form the stack pattern (10 PZT nano ribbons connected in parallel in one module and 3 × 4 moduli connected in series) [27]. Then the functional part was transfer-printed to polyimide thin film (thickness ~ 50 µm, $E = 2.83$ GPa), which serves as the soft bottom substrate layer. At last, the device is connected to a flexible anisotropic conductive film cable (figure 1*b*). To investigate the *in vivo* biomechanical energy harvesting efficiency, we integrated the device on the heart surface of experimental swine (figure 1*c*). The swine in the experiment was handled with the permission from the Ethics Committee. When the porcine heart was beating, the flexible PZT MEH was forced to deform, and the output voltage of the device was measured by an AD/DA card and transmitted to a computer for further analyses.

As the outer LV is a curved surface, the device, when sewed at the LV surface by its two ends, is subjected to bending deformation with large deflections (figure 1*d*) during the heart motion in experiment [27]. The PZT nano ribbons are much more compliant than the substrate, and,

therefore, the contribution of the PZT nano ribbons to the bending and stretching rigidity of the device is neglected. During the cardiac systole and diastole process, the device is forced to deform periodically. Neglecting the initial curvature of the device due to the LV surface, the deformation of the device is governed by

$$E_s I_s \frac{d^4 w}{d^4 x} + N_0 \frac{d^2 w}{dx^2} = 0, \tag{2.1}$$

among which $N_0 = E_s A_s[(du_0/dx) + 1/2(dw/dx)^2]$ is the constant membrane force due to large deflection of the device, w is the deflection and u_0 is the in-plane displacement at the neutral axis, while E_s, A_s and I_s are, respectively, the elastic modulus, area and moment of inertia of the substrate.

According to anatomy, there exists a small space ($A_c = 5$–10 mm [29]) between the left lung and the heart, this may accommodate free deformation of the device when the deformation amplitude $A < A_c$. However, the lung will pose an impedance effect on the device as $A \geq A_c$, and thus, the output voltage is reduced. Therefore, the boundary conditions for the governing equation (2.1) will depend on the relationship between the deformation amplitude A and the permitted space A_c.

(a) Free deformation ($A < A_c$)

At the free deformation stage ($A \leq A_c$), the MEH device is only constrained at its sewed ends with an end-to-end displacement of ΔL. The sewed ends are regarded as in clamped condition (figure 1*d*) to satisfy

$$\left.\begin{aligned} w|_{x=\pm L_0/2} &= \left.\frac{dw}{dx}\right|_{x=\pm L_0/2} = 0 \\ \text{and} \quad u_0|_{x=\pm L_0/2} &= \mp \frac{\Delta L}{2}, \end{aligned}\right\} \tag{2.2}$$

The general solutions for the governing differential equation (2.1) are

$$w = c_1 \cos(\alpha_1 x) + c_2 \sin(\alpha_1 x) + c_3 x + c_4 \tag{2.3}$$

and

$$u_0 = \frac{N_0}{E_s A_s} x + \left(\frac{c_1 \alpha_1}{2}\right)^2 \left[\frac{1}{2\alpha_1} \sin(2\alpha_1 x) - x\right] + c_5, \tag{2.4}$$

where $\alpha_1 = \sqrt{N_0/(E_s I_s)}$ is the eigenvalue of equation (2.1) and c_i are unknown constants.

Upon incorporating the boundary conditions in equation (2.2), the non-zero parameters in (2.3) and (2.4) are obtained as $c_1 = c_4 = (L_0/\pi)\sqrt{(\Delta L/L_0) - (4\pi^2/L_0^2)(I_s/A_s)}$, $\alpha_1 = 2\pi/L_0$ and $N_0 = (4\pi^2/L_0^2)E_s I_s$. During the systole of the heart, the relative end-to-end displacement of the device $\Delta L/L_0$ (approx. 10^{-1}) is much larger than the membrane strain $(4\pi^2/L_0^2)(I_s/A_s)$ (approx. 10^{-5}); therefore, the displacements are derived as

$$\left.\begin{aligned} w &= \frac{L_0}{\pi}\sqrt{\frac{\Delta L}{L_0}}\left[1 + \cos\left(\frac{2\pi x}{L_0}\right)\right] \\ \text{and} \quad u_0 &= \frac{\Delta L}{L_0}\left[\frac{L_0}{4\pi}\sin\left(\frac{4\pi x}{L_0}\right) - x\right], \end{aligned}\right\} \tag{2.5}$$

from which the deflection amplitude is $A = (2/\pi)\sqrt{L_0 \Delta L}$. This solution is identical to the traditional empirical results based on the post-buckling analyses [30,31]. The axial strain in the PZT ribbon is $\varepsilon_{PZT} = -(E_s I_s/\overline{EI}) z_p (d^2 w/dx^2)$, where $\overline{EI}$ and z_p are, respectively, the effective bending stiffness and the distance from the centre of the PZT ribbons to the neutral axis of the composite part of the device. As the PZT ribbons are integrated near the substrate centre, and

their lengths (approx. 2 mm) are much shorter than the substrate (approx. 50 mm), the average strain of the PZT ribbons may be approximated as

$$\varepsilon_{\mathrm{PZT}} = 4\pi \frac{E_{\mathrm{s}} I_{\mathrm{s}}}{\overline{EI}} \frac{z_{\mathrm{p}}}{L_0} \sqrt{\frac{\Delta L}{L_0}}. \tag{2.6}$$

(b) Constrained deformation ($A \geq A_{\mathrm{c}}$)

When undergoing a large deformation ($A > A_{\mathrm{c}}$) during the systole of the heart, the MEH device will contact with the surrounding tissues at the centre part. Here, the adhesion effect between the MEH device and the surrounding tissues is neglected, then the contact length will be zero [32,33], that is, the device will have only the centre point contacting with the surround tissues. For simplicity, the deformation of the surrounding tissues is further ignored or the surrounding tissues are assumed rigid when compared with the MEH device, then the displacement and the slope at the device centre will keep at $w|_{x=0} = A_{\mathrm{c}}$ and $w'|_{x=0} = 0$. Combining these constraint conditions and the symmetric nature of the device ($u_0|_{x=0} = 0$) with the boundary conditions in equation (2.2), the non-zero unknown constants c_i are determined by

$$\left.\begin{aligned} c_1 &= \frac{1-\cos\lambda}{2-2\cos\lambda-\lambda\sin\lambda} A_{\mathrm{c}},\ c_2 = \frac{-\sin\lambda}{2-2\cos\lambda-\lambda\sin\lambda} A_{\mathrm{c}} \\ c_3 &= \frac{2\lambda\sin\lambda}{2-2\cos\lambda-\lambda\sin\lambda} \frac{A_{\mathrm{c}}}{L_0},\ c_4 = \frac{1-\cos\lambda-\lambda\sin\lambda}{2-2\cos\lambda-\lambda\sin\lambda} A_{\mathrm{c}}, \end{aligned}\right\} \tag{2.7}$$

and the membrane force is $N_0 = 4E_{\mathrm{s}}I_{\mathrm{s}}(\lambda^2/L_0^2)$, where $\lambda = \alpha_1 L_0/2$ is the root of the following characteristic equation,

$$\lambda^2 \left(\frac{1-\cos\lambda}{2-2\cos\lambda-\lambda\sin\lambda}\right)^2 \left(\frac{\sin 2\lambda}{2\lambda} - 1\right) + \frac{\pi^2}{4}\left(\frac{A}{A_{\mathrm{c}}}\right)^2 = 0. \tag{2.8}$$

The average strain of the PZT ribbons may be approximated as

$$\varepsilon_{\mathrm{PZT}} \approx \frac{E_{\mathrm{s}} I_{\mathrm{s}}}{\overline{EI}} z_{\mathrm{p}} c_1 \alpha_1^2 = 4 \frac{E_{\mathrm{s}} I_{\mathrm{s}}}{\overline{EI}} \frac{z_{\mathrm{p}}}{L_0} \frac{A_{\mathrm{c}}}{L_0} \frac{\lambda^2(1-\cos\lambda)}{2-2\cos\lambda-\lambda\sin\lambda}. \tag{2.9}$$

Noted that we have $\lambda = \pi$ when $A_{\mathrm{c}} = A$, then the solution in equation (2.9) may be reduced to equation (2.6) for the case of $A < A_{\mathrm{c}}$.

3. Electric outputs of the mechanical energy harvester device

According to the electromechanical coupling behaviour of piezoelectric materials and following the previous analyses [28], the governing equation for total output voltage V_{total} of the MEH device with an electrical resistance R is

$$\frac{\mathrm{d}V_{\mathrm{total}}}{\mathrm{d}t} + \frac{n_{\mathrm{s}} h_{\mathrm{p}}}{n_{\mathrm{p}} \bar{\mu}_{33} A_{\mathrm{p}} R} V_{\mathrm{total}} = -\frac{n_{\mathrm{s}} \bar{e}_{31} h_{\mathrm{p}}}{\bar{\mu}_{33}} \frac{\mathrm{d}\varepsilon_{\mathrm{PZT}}}{\mathrm{d}t}, \tag{3.1}$$

where n_{p} and n_{s} are the number of PZT ribbons connected in parallel and the number of moduli connected in series, h_{p} and A_{p} are the thickness and area of each individual PZT ribbon, while $\bar{e}_{31}$ and $\bar{\mu}_{33}$ are, respectively, the effective piezoelectric and dielectric constants of the PZT ribbons. The total output voltage from equation (3.1) with the initial condition $V_{\mathrm{total}}(0) = 0$ is

$$V_{\mathrm{total}}(t) = -\frac{n_{\mathrm{s}} \bar{e}_{31} h_{\mathrm{p}}}{\bar{\mu}_{33}} \int_0^t \exp\left[-\frac{n_{\mathrm{s}} h_{\mathrm{p}} (t-t')}{n_{\mathrm{p}} \bar{\mu}_{33} A_{\mathrm{p}} R}\right] \frac{\mathrm{d}\varepsilon_{\mathrm{PZT}}}{\mathrm{d}t'} \mathrm{d}t'. \tag{3.2}$$

Equations (3.2) and (2.9) or (2.6) indicate that the output voltage of the MEH device may be calculated once the real-time end-to-end displacement of the device $\Delta L(t)$ is known.

For the current energy harvesting from heartbeat by sewing the MEH device at the LV surface, the end-to-end displacement $\Delta L(t)$, according to the assumption of bullet-shape or ellipsoid-shape [34], may be determined by $\Delta L(t)/L_0 = [D_{\mathrm{diastolic}} - D(t)]/[D_{\mathrm{diastolic}} + 2t_{\mathrm{wall}}]$, where t_{wall},

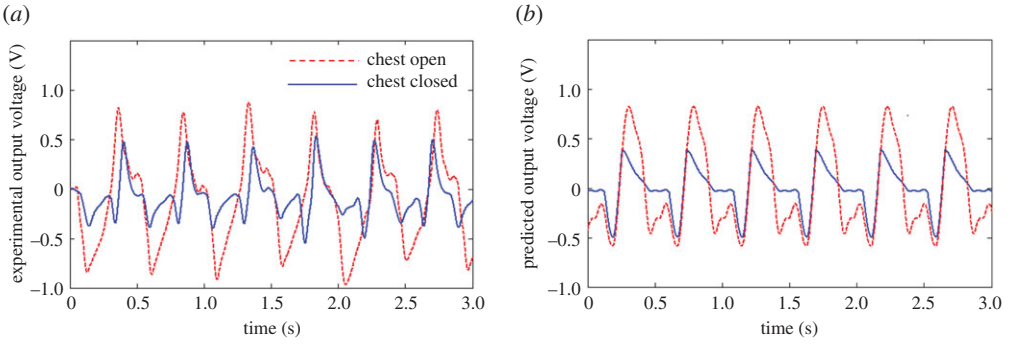

Figure 2. Output voltage of the MEH when the chest is open and closed. (*a*) Experimental output voltage. (*b*) Predicted output voltage based on the analytical model. (Online version in colour.)

$D_{\text{diastolic}}$ and $D(t)$ are, respectively, the wall thickness, diastolic and the real-time minor axis diameter of the LV. The real-time minor axis diameter $D(t)$ is related to the volume of the LV by $V_{\text{LV}} = 7.0D^3(t)/[2.4 + D(t)]$ [35]. As the real-time LV volume V_{LV} of swine is not available, we will use the corresponding *in vivo* data of human heart [36] to approximate the porcine LV due to their similar cardiac physiology [37–39]. The main difference between the real-time LV volume V_{LV} of human and swine is the cardiac period, which makes it necessary to scale the cardiac period of human heart to the porcine heart in experiment.

The current PZT MEH device in the experiment contains 12 moduli connected in series with each module containing 10 PZT nano ribbons ($h_{\text{p}} = 0.5\,\mu\text{m}$, $A_{\text{p}} = 0.22\,\text{mm}^2$) connected in parallel. The effective piezoelectric $\bar{e}_{31}$ and dielectric constants $\bar{\mu}_{33}$ of the PZT nano ribbon are $-6.2\,\text{C m}^{-2}$ and $2 \times 10^{-8}\,\text{C/(Vm)}$ [40], respectively. Using the loading condition generated by the above analogy, the predicted real-time output voltages with chest open and closed ($A_{\text{C}} = 6.5\,\text{mm}$, figure 2*b*) exhibit a reduction of about 40% in the peak-to-valley voltage, which is generally consistent with experiments (figure 2*a*). This demonstrates the capability of the current theoretical model to reveal the underlying mechanism of reduction in voltage output by the MEH device in chest closed environment.

The energy harvesting efficiency is the foremost concern that determines the feasibility of the MEH device for practical applications to power biointegrated or implanted microdevices. Normally, the effective output power $P_{\text{eff}} = V_{\text{eff}}^2/R$ is used to evaluate the efficiency of the MEH device, where $V_{\text{eff}} = \sqrt{\left(\int_0^T V_{\text{total}}^2 \text{d}t\right)/T}$ is the root of mean squares of the output voltage, or termed as the effective voltage. Theoretical predictions exhibit that the effective output power P_{eff} increases monotonically with the permitted space A_{c} until it exceeds a certain value that will not pose impeding effects on the device (figure 3). Correspondingly, the effective output power will have a larger reduction $(P_{\text{eff}}^{\text{free}} - P_{\text{eff}})/P_{\text{eff}}^{\text{free}}$ for smaller permitted space. The predicted output power is 0.021 µW for chest open and 0.005 µW for chest closed with a permitted space $A_{\text{C}} = 6.5\,\text{mm}$ (with a reduction of 76%), which are identical to the experimental measurements, 0.02 and 0.005 µW with chest open and closed (with a reduction of 75%) [27].

In the chest closed environment, respiration may induce elastic deformation or volume change of the lung [41], and, hence, the timely variation of the pleural cavity or permitted space A_{C}. The porcine cardiac rate is about 120–140 beats min^{-1} [41], while the respiratory rate is about 20 times min^{-1} [42]. Sinusoidal expiratory flow is usually used for studying lung mechanical properties [43], then we assume $A_{\text{C}} = A_{\text{C0}} + A_{\text{C1}}\sin(\omega_{\text{r}}t)$, where $A_{\text{C0}} = 6.5\,\text{mm}$ is the average permitted space [29], while A_{C1} and ω_{r} are, respectively, the amplitude and frequency of the resonant space. According to the typical statistics of normal adult lung during respiration, these two parameters may be obtained approximately as $A_{\text{C1}} = 3.0\,\text{mm}$ and $\omega_{\text{r}} = 2.1\,\text{rad s}^{-1}$ [43]. Theoretical results of the real-time output voltage again agree very well with experiments (figure 4), indicating

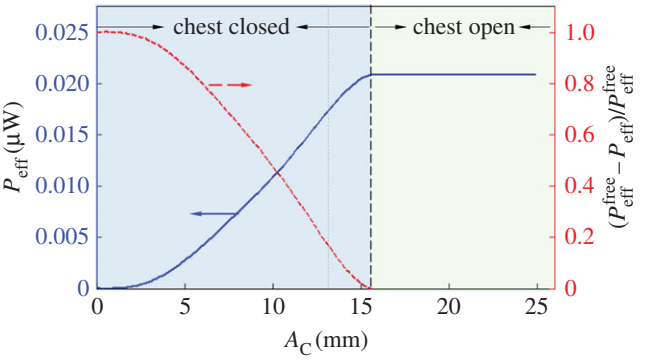

Figure 3. The electric power P_{eff} and its relative decrement $(P_{\text{eff}}^{\text{free}} - P_{\text{eff}})/P_{\text{eff}}^{\text{free}}$ against the permitted space A_{C}. (Online version in colour.)

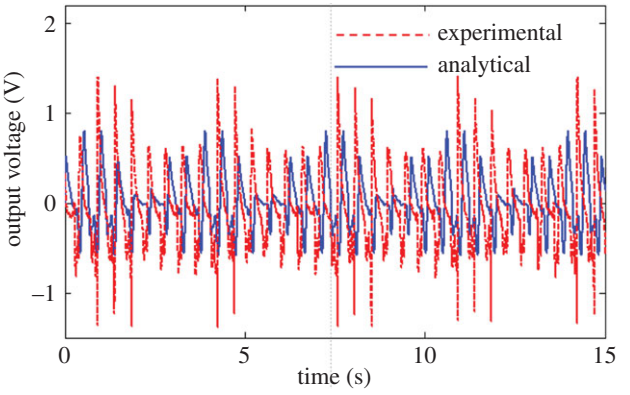

Figure 4. Comparisons of the predicted output voltage including the effects of respiration with experiments. (Online version in colour.)

that the current theoretical model is robust for predicting energy harvesting from heartbeat in practical living environment. The result is also inspiring for potential applications in respiratory monitoring, for example, to retrieve real-time respiratory rate and respiratory intensity.

4. Scaling laws for energy harvesting

Multiple parameters, including material parameters (e.g. piezoelectric constant $\bar{e}_{31}$, dielectric constant $\bar{\mu}_{33}$, Young's modulus of the substrate E_{s} and the effective modulus of the whole device $\bar{E}$), geometrical parameters (e.g. length of the device L_0, thickness and effective area of the PZT ribbon h_{p} and A_{p}, thickness of the substrate h_{s}, moment of inertia of the substrate I_{s}, effective moment of inertia of the whole device $\bar{I}$, the distance from the centre of the PZT layer to the centre of the PZT MEH z_{p}, and the permitted space A_{C}), circuit parameters (e.g. number of PZT ribbons n_{p} connected in parallel in one module, number of energy harvesting moduli n_{s} connected in series and electrical load of the circuit R) and loading parameters (e.g. the real-time end-to-end displacement ΔL, the period of heartbeat T and the respiration rate ω_{r}), are contained in the output voltage V_{total} given in equation (3.2). This makes the investigation of the effects of each individual parameter on the energy harvesting efficiency intricate and complex. To investigate the intrinsic effects of these parameters on the energy harvesting efficiency from heartbeat, we will establish simple scaling laws to reveal the underlying physics and links between the electric outputs and various parameters.

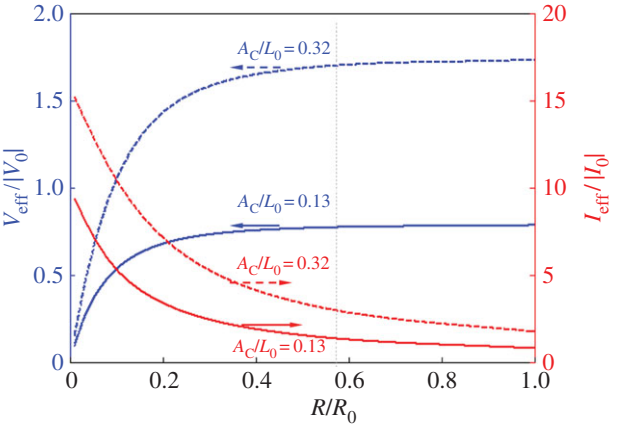

Figure 5. Scaling law for the normalized effective voltage $V_{eff}/|V_0|$ and normalized effective current $I_{eff}/|I_0|$for chest open ($A_C/L_0 = 0.32$) and closed ($A_C/L_0 = 0.13$) against the normalized circuit load R/R_0. (Online version in colour.)

To this end, we introduce the intrinsic scales of voltage $V_0 = (E_s I_s/\overline{EI})(n_s \bar{e}_{31} h_p z_p/\bar{\mu}_{33} L_0)$, time $t_0 = n_p \bar{\mu}_{33} A_p R/n_s h_p$ or electrical load $R_0 = n_s h_p T/n_p \bar{\mu}_{33} A_p$, and then the normalized real-time output voltage including the effects of limited space may be expressed as

$$\frac{V_{total}}{V_0} = \bar{V}_{total}\left(\frac{t}{t_0}, \frac{R}{R_0}, \frac{\Delta L_{max}}{L_0}, \frac{A_c}{L_0}\right), \tag{4.1}$$

when $\Delta L_{max}/L_0$ is the normalized maximal end-to-end displacement of the device, and, for a healthy adult heart, this parameter is statistically constant of $\Delta L_{max}/L_0 \approx 0.25$ [36]. Accordingly, the scaling laws for the normalized electric outputs are obtained as

$$\frac{\varphi_{eff}}{\varphi_0} = \bar{\varphi}_{eff}\left(\frac{R}{R_0}, \frac{A_c}{L_0}\right), \tag{4.2}$$

where φ can either be the output voltage V, output current I or output power P, while V_0, $I_0 = (E_s I_s/\overline{EI})(n_p \bar{e}_{31} z_p A_p/L_0 T)$ and $P_0 = ((E_s I_s/\overline{EI})(\bar{e}_{31} z_P/L_0))^2 (n_s n_p A_p h_p/\bar{\mu}_{33} T)$ are, respectively, the intrinsic scales of current and power. The scaling law in equation (4.2) indicates that the normalized electric outputs (voltage, current, power or power density) only depend on two combined parameters, i.e. the normalized electrical load R/R_0 and the normalized permitted space A_c/L_0.

Figures 5 and 6 present the dependence of the normalized effective voltage V_{eff}/V_0, the normalized effective current I_{eff}/I_0 and the normalized effective power P_{eff}/P_0 on the normalized electrical load R/R_0 in the energy harvesting circuit for various normalized permitted space A_C/L_0. The normalized output voltage V_{eff}/V_0 increases monotonically with R/R_0 and tends to saturate for large electrical load with the limit corresponding to the case of open circuit voltage (figure 5). In comparison, the normalized output current I_{eff}/I_0 decreases monotonically with R/R_0 and approaches zero for large electrical load, corresponding to the case of open circuit current. When the electrical load is zero, the energy harvesting circuit is short connected, resulting in a zero voltage and large current. For both the two extreme cases, the effective output power is zero which indicates that the MEH device does not harvest any electrical energy. For a practical energy harvesting circuit, the output power P_{eff}/P_0 attains the maximum as $R/R_0 = 0.130$ (figure 6), nearly identical to $1/2\pi$ for the energy harvesting from harmonic motions [44]. The scaling law presented in the form of figure 6 is helpful to optimize the efficiency of energy harvester by selecting properly the electric load for the circuit or other system parameters. For example, for an MEH device with a fixed total number of PZT ribbons and moduli (n_s n_p is fixed), there exists an optimal ratio of n_p/n_s to deliver a maximal output power. The optimal

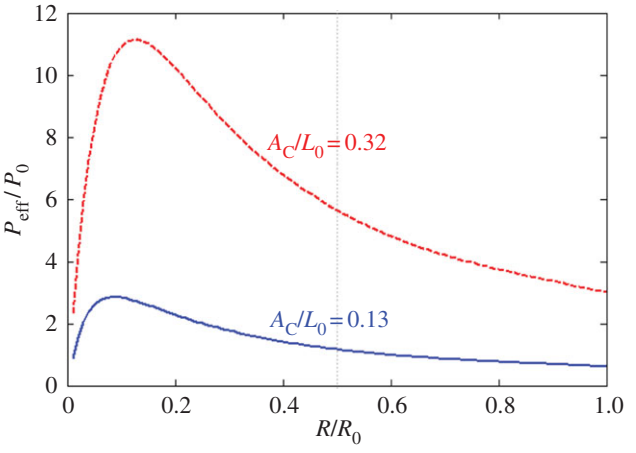

Figure 6. Scaling law for the normalized output power P_{eff}/P_0 for chest open ($A_C/L_0 = 0.32$) and closed ($A_C/L_0 = 0.13$) against the normalized circuit load R/R_0. (Online version in colour.)

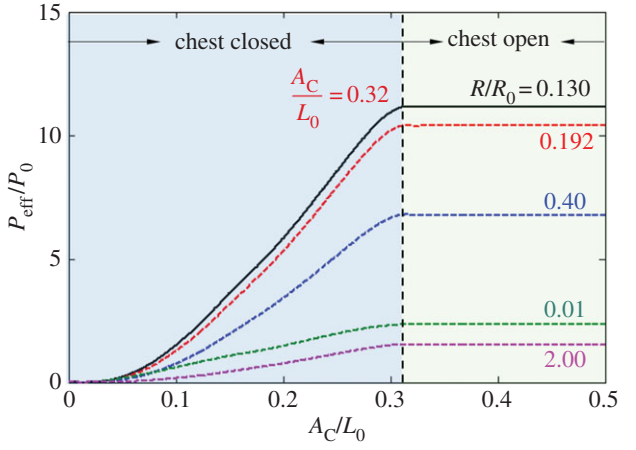

Figure 7. Scaling law for the normalized output power P_{eff}/P_0 against the normalized permit space A_c/L_0 for various normalized circuit loads R/R_0. (Online version in colour.)

output power may also be realized by designing the geometry of the PZT ribbon (a proper A_p/h_p) once the volume $A_p h_p$ of the ribbon is given (figure 6).

The scaling laws (figures 5 and 6) also reveal the adverse effects of the limited permitted space A_C/L_0 on the efficiency of the MEH device. The smaller the permitted space is, the lower output power is achieved (figure 6). According to the physiology of heart motion, the resulted maximal end-to-end displacement of the device is $\Delta L_{max}/L_0 \approx 0.25$ [36], which can be substituted into the deflection amplitude in equation (2.5) leading to the maximal amplitude as $A_{max}/L_0 = 0.32$. This indicates that the device will behave like the case of free deformation as the permitted space $A_C/L_0 > 0.32$. Thus, the normalized output power P_{eff}/P_0 keeps increasing until A_C/L_0 exceeds 0.32 where the power remains constant and is equal to the case of chest open (figure 7). The effective power produced by the energy harvesting system in the experiment ($R/R_0 = 0.192$) is a little bit lower than the optimal case $R/R_0 = 0.130$. The scaling law presented in the form of figure 7 may also provide guidelines for designing the MEH device to achieve as higher output power as possible. Combining the investigations on equation (2.9) and the $P_{eff}/P_0 \sim A_C/L_0$ curve

in figure 7, the output power is inversely proportional to at least the fourth order of the device length L_0, that is, shorter devices (smaller L_0) may produce higher output power. Taking the device in experiment ($R/R_0 = 0.192$, $L_0 = 5.0$ cm), for example, the effective output power P_{eff} may increase up to 2.5 times if the device length decreases by 20% ($L_0 = 4.0$ cm). Even if the device is so short that the relative permitted space satisfies $A_C/L_0 > 0.32$, the output power will keep inversely proportional to the square of the device length L_0. The scaling law also implies that the output power is proportional to the square of the bending rigidity ratio $E_sI_s/\overline{EI}$, effective piezoelectric constant $\bar{e}_{31}$ and the distance z_p of the PZT ribbons away from the neutral axis of the device.

5. Conclusion

We have developed a restricted-space deformation model to predict the efficiency of energy harvesting from the heartbeat using flexible PZT devices. The model was validated by comparing analytical results to experimental measurements, which demonstrated its capability of revealing the underlying mechanism of reduction in the efficiency of energy harvesting in chest closed environment compared to the case of chest open. A simple scaling law for the energy harvesting from heartbeat is established in terms of material, geometric, circuit and heartbeat parameters. The normalized power output by the energy harvesting system only depends on two combined parameters, i.e. the normalized pleural cavity and the normalized electrical load of the circuit. With prescribed PZT ribbons and energy harvesting moduli, the most efficient means of increasing the energy harvesting efficiency is to select proper electrical load and decrease the device length. The results may serve as guidelines for optimization of energy harvesting from heartbeat or the motion of other biological organs.

Ethics. All *in vivo* experiments performed were approved by the Ethics Committee (Ethics Committee of Beijing Anzhen Hospital, Capital University of Medical Sciences) and in accordance with relevant guidelines and regulations. Experimental swine raised especially for cardiovascular research are selected for *in vivo* testing.

Data accessibility. The datasets supporting the conclusions are accessible in the article.

Authors' contributions. Y.Z. carried out the analytic modelling, analysed the data and drafted the manuscript; C.L. designed the analytic model, analysed the data, revised and finalized the manuscript. B.L. and X.F. provided the experimental data and photos.

Competing interests. We declare we have no competing interests.

Funding. C.L. acknowledges the financial supports by the National Natural Science Foundation of China at grant nos 11322216 and 11621062. X.F. acknowledges the supports by the National Natural Science Foundation of China at grant no. 11320101001. B.L. acknowledges the support of the National Natural Science Foundation of China at grant no. 11502126.

Acknowledgements. The authors thank the reviewers for their helpful comments and suggestions for improving this article.

References

1. Lohmeier TE, Iliescu R, Liu B, Henegar JR, Maricbilkan C, Irwin ED. 2012 Systemic and renal-specific sympathoinhibition in obesity hypertension. *Hypertension* **59**, 331–338. (doi:10.1161/hypertensionaha.111.185074)
2. Kobayashi M, Massiello A, Karimov JH, Van Wagoner DR, Fukamachi K. 2013 Cardiac autonomic nerve stimulation in the treatment of heart failure. *Ann. Thorac. Surg.* **96**, 339–345. (doi:10.1016/j.athoracsur.2012.12.060)
3. Potkay JA. 2008 Long term, implantable blood pressure monitoring systems. *Biomed. Microdevices* **10**, 379–392. (doi:10.1007/s10544-007-9146-3)
4. Lavan DA, Mcguire T, Langer R. 2003 Small-scale systems for *in vivo* drug delivery. *Nat. Biotechnol.* **21**, 1184–1191. (doi:10.1038/nbt876)
5. Rak-Hwan K *et al.* 2012 Flexible electronics: materials and designs for wirelessly powered implantable light-emitting systems. *Small* **8**, 2812–2818. (doi:10.1002/smll.201200943)
6. Mond HG, Proclemer A. 2011 The 11th world survey of cardiac pacing and implantable cardioverter-defibrillators: calendar year 2009—a World Society of Arrhythmia's project. *PACE* **34**, 1013–1027. (doi:10.1111/j.1540-8159.2011.03150.x)

7. Poole JE *et al.* 2010 Complication rates associated with pacemaker or implantable cardioverter-defibrillator generator replacements and upgrade procedures: results from the REPLACE registry. *Circulation* **122**, 1553–1561. (doi:10.1161/circulationaha.110.976076)
8. Kim KH, Lee KY, Seo JS, Kumar B, Kim SW. 2011 Paper-based piezoelectric nanogenerators with high thermal stability. *Small* **7**, 2577–2580. (doi:10.1002/smll.201100819)
9. Bowen CR, Kim HA, Weaver PM, Dunn S. 2013 Piezoelectric and ferroelectric materials and structures for energy harvesting applications. *Energy Environ. Sci.* **7**, 25–44. (doi:10.1039/c3ee42454e)
10. Yang Y, Zhang H, Chen J, Lee S, Hou TC, Wang ZL. 2013 Simultaneously harvesting mechanical and chemical energies by a hybrid cell for self-powered biosensors and personal electronics. *Energy Environ. Sci.* **6**, 1744–1749. (doi:10.1039/c3ee40764k)
11. Lee JH, Lee KY, Kumar B, Tien NT, Lee NE, Kim SW. 2012 Highly sensitive stretchable transparent piezoelectric nanogenerators. *Energy Environ. Sci.* **6**, 169–175. (doi:10.1039/c2ee23530g)
12. Antoine GO, De LE, Michelin S. 2016 Optimal energy harvesting from vortex-induced vibrations of cables. *Proc. R. Soc. A* **472**, 20160583. (doi:10.1098/rspa.2016.0583)
13. Renzi E. 2017 Hydroelectromechanical modelling of a piezoelectric wave energy converter. *Proc. R. Soc. A* **472**, 20160715. (doi:10.1098/rspa.2016.0715)
14. Rogers JA, Someya T, Huang Y. 2010 Materials and mechanics for stretchable electronics. *Science* **327**, 1603–1607. (doi:10.1126/science.1182383)
15. Ma Y, Xue Y, Jang KI, Feng X, Rogers JA, Huang Y. 2016 Wrinkling of a stiff thin film bonded to a pre-strained, compliant substrate with finite thickness. *Proc. R. Soc. A* **472**, 20160339. (doi:10.1098/rspa.2016.0339)
16. Khang D-Y, Jiang H, Huang Y, Rogers JA. 2006 A stretchable form of single-crystal silicon for high-performance electronics on rubber substrates. *Science* **311**, 208–212. (doi:10.1126/science.1121401)
17. Kim DH *et al.* 2008 Materials and noncoplanar mesh designs for integrated circuits with linear elastic responses to extreme mechanical deformations. *Proc. Natl Acad. Sci. USA* **105**, 18 675–18 680. (doi:10.1073/pnas.0807476105)
18. Zhang Y, Fu H, Su Y, Xu S, Cheng H, Fan JA, Hwang KC, Rogers JA, Huang Y. 2013 Mechanics of ultra-stretchable self-similar serpentine interconnects. *Acta Mater.* **61**, 7816–7827. (doi:10.1016/j.actamat.2013.09.020)
19. Dagdeviren C *et al.* 2014 Conformal piezoelectric energy harvesting and storage from motions of the heart, lung, and diaphragm. *Proc. Natl Acad. Sci. USA* **111**, 1927–1932. (doi:10.1073/pnas.1317233111)
20. Ansari MH, Karami MA. 2017 Experimental investigation of fan-folded piezoelectric energy harvesters for powering pacemakers. *Smart Mater. Struct.* **26**, 065001. (doi:10.1088/1361-665X/aa6cfd)
21. Wang ZL, Song J. 2006 Piezoelectric nanogenerators based on zinc oxide nanowire arrays. *Science* **312**, 242–246. (doi:10.1126/science.1124005)
22. Hwang GT *et al.* 2014 Self-powered cardiac pacemaker enabled by flexible single crystalline PMN-PT piezoelectric energy harvester. *Adv. Mater.* **26**, 4880–4887. (doi:10.1002/adma.201400562)
23. Chang C, Tran VH, Wang J, Fuh YK, Lin L. 2010 Direct-write piezoelectric polymeric nanogenerator with high energy conversion efficiency. *Nano Lett.* **10**, 726–731. (doi:10.1021/nl9040719)
24. Zhang H *et al.* 2015 A flexible and implantable piezoelectric generator harvesting energy from the pulsation of ascending aorta: *in vitro* and *in vivo* studies. *Nano Energy* **12**, 296–304. (doi:10.1016/j.nanoen.2014.12.038)
25. Zheng Q *et al.* 2014 *In vivo* powering of pacemaker by breathing-driven implanted triboelectric nanogenerator. *Adv. Mater.* **26**, 5851–5856. (doi:10.1002/adma.201402064)
26. Wang ZL, Chen J, Lin L. 2015 Progress in triboelectric nanogenerators as a new energy technology and self-powered sensors. *Energy Environ. Sci.* **8**, 2250–2282. (doi:10.1039/c5ee01532d)
27. Lu B *et al.* 2015 Ultra-flexible piezoelectric devices integrated with heart to harvest the biomechanical energy. *Sci. Rep.* **5**, 16065. (doi:10.1038/srep16065)
28. Zhang Y, Chen Y, Lu B, Lü C, Feng X. 2016 Electromechanical modeling of energy harvesting from the motion of left ventricle in closed chest environment. *J. Apll. Mech-T. ASME* **83**, 061007. (doi:10.1115/1.4032994)

29. Ferguson MK. 2007 *Thoracic surgery atlas*. Philadelphia, PA: Saunders Elsevier.
30. Li Y, Song J, BoFang, Zhang J. 2011 Surface effects on the postbuckling of nanowires. *J. Phys. D. Appl. Phys.* **44**, 425304. (doi:10.1088/0022-3727/44/42/425304)
31. Vella D, Bico J, Boudaoud A, Roman B, Reis PM. 2009 The macroscopic delamination of thin films from elastic substrates. *Proc. Natl Acad. Sci. USA* **106**, 10 901–10 906. (doi:10.1073/pnas.0902160106)
32. Yang F. 2003 Contact deformation of a micromechanical structure. *J. Micromech. Microeng.* **14**, 263–268. (doi:10.1088/0960-1317/14/2/014)
33. Lü C, Wu D, Chen W. 2011 Surface effects on the jump-in instability of nanomechanical structures. *IEEE Trans. Nanotechnol.* **10**, 962–967. (doi:10.1109/tnano.2010.2091422)
34. Lang RM *et al.* 2005 Recommendations for chamber quantification. *J. Am. Soc. Echocardiogr.* **18**, 1440–1463. (doi:10.1016/j.echo.2005.10.005)
35. Teichholz LE, Kreulen T, Herman MV, Gorlin R. 1976 Problems in echocardiographic volume determinations: echocardiographic-angiographic correlations in the presence of absence of asynergy. *Am. J. Cardiol.* **37**, 7–11. (doi:10.1016/0002-9149(76)90491-4)
36. Corsi C, Saracino G, Sarti A, Lamberti C. 2002 Left ventricular volume estimation for real-time three-dimensional echocardiography. *IEEE Trans. Med. Imaging.* **21**, 1202–1208. (doi:10.1109/tmi.2002.804418)
37. Hill AJ, Laske Jr TG, Sigg DC, Skadsberg ND, Vincent SA, Soule CL, Gallagher WJ, Iaizzo PA. 2005 *In vitro* studies of human hearts. *Ann. Thorac. Surg.* **79**, 168–177. (doi:10.1016/j.athoracsur.2004.06.080)
38. Sigg DC, Iaizzo PA. 2006 *In vivo* versus *in vitro* comparison of swine cardiac performance: induction of cardiodepression with halothane. *Eur. J. Pharmacol.* **543**, 97–107. (doi:10.1016/j.ejphar.2006.06.011)
39. Mohiuddin MM, Reichart B, Byrne GW, Mcgregor CG. 2015 Current status of pig heart xenotransplantation. *Int. J. Surg.* **23**, 234–239. (doi:10.1016/j.ijsu.2015.08.038)
40. Su Y, Dagdeviren C, Li R. 2015 Measured output voltages of piezoelectric devices depend on the resistance of voltmeter. *Adv. Funct. Mater.* **25**, 5320–5325. (doi:10.1002/adfm.201502280)
41. Liedtke AJ, Nellis S, Neely JR. 1978 Effects of excess free fatty acids on mechanical and metabolic function in normal and ischemic myocardium in swine. *Circ. Res.* **43**, 652–661. (doi:10.1161/01.RES.43.4.652)
42. Heitman Jr H, Hughes EH. 1949 The effects of air temperature and relative humidity on the physiological well being of swine. *J. Anim. Sci.* **8**, 171–181. (doi:10.2527/jas1949.82171x)
43. Bitzén U, Niklason L, Göransson I, Jonson B. 2010 Measurement and mathematical modelling of elastic and resistive lung mechanical properties studied at sinusoidal expiratory flow. *Clin. Physiol. Funct. Imaging*, **30**, 439–446. (doi:10.1111/j.1475-097X.2010.00963.x)
44. Lu F, Lim SP, Lee HP. 2003 Modeling and analysis of micro piezoelectric power generators for micro-electromechanical-systems applications. *Smart Mater. Struct.* **13**, 57–63. (doi:10.1088/0964-1726/13/1/007)